



**HAL**  
open science

## **Influence of micro-structural features on the colour of nanocrystallised powders of hematite and visible-NIR reflectance spectra simulations**

Morgane Gerardin, Nicolas Holzschuch, Alain Ibanez, Bernard Schmitt,  
Pauline Martinetto

### ► To cite this version:

Morgane Gerardin, Nicolas Holzschuch, Alain Ibanez, Bernard Schmitt, Pauline Martinetto. Influence of micro-structural features on the colour of nanocrystallised powders of hematite and visible-NIR reflectance spectra simulations. *Journal of the international colour association*, 2021, 26, pp.41-48. hal-03174514

**HAL Id: hal-03174514**

**<https://hal.science/hal-03174514v1>**

Submitted on 19 Mar 2021

**HAL** is a multi-disciplinary open access archive for the deposit and dissemination of scientific research documents, whether they are published or not. The documents may come from teaching and research institutions in France or abroad, or from public or private research centers.

L'archive ouverte pluridisciplinaire **HAL**, est destinée au dépôt et à la diffusion de documents scientifiques de niveau recherche, publiés ou non, émanant des établissements d'enseignement et de recherche français ou étrangers, des laboratoires publics ou privés.

# Influence of micro-structural features on the colour of nanocrystallised powders of hematite and visible-NIR reflectance spectra simulations

Morgane Gerardin<sup>†</sup>, Nicolas Holzschuch, Alain Ibanez<sup>\*</sup>, Bernard Schmitt<sup>#</sup> and Pauline Martinetto<sup>\*</sup>

*Univ. Grenoble Alpes, CNRS, Inria, Grenoble INP, LJK, 38000 Grenoble, France*

*\*Univ. Grenoble Alpes, CNRS, Institut Néel, 38000 Grenoble, France*

*#Univ. Grenoble Alpes, CNRS, IPAG 38000 Grenoble, France*

*†Email: gerardin.morgane@gmail.com*

Pigments are quite complex materials whose appearance involves many optical phenomena. Here, we focused on hematite as it is a traditional pigment, whose origin of coloration has been well discussed in the literature. Pure nanocrystallised  $\alpha$ -Fe<sub>2</sub>O<sub>3</sub> hematite powders have been synthesised using different synthesis routes. These powders have been characterised by X-ray powder diffraction and scanning electronic microscopy. The colour of the samples has been studied by visible-NIR spectrophotometry. We obtained hematite with both various grain morphologies and noticeably different shades going from orange-red to purple. Colorimetric parameters in CIE L\*a\*b\* colour space and diffuse reflectance spectra properties were studied against the structural parameters. For small nanocrystals, hue is increasing with the grain size until a critical diameter of about 80 nm, where the trend is reversed. Since classical scattering theories are not able to model this trend, we believe a combination of multiple physical phenomena occurring at this scale may explain it.

*Received 22 January 2021; accepted 01 February 2021*

*Published online: 16 February 2021*

## Introduction

Pigments are quite complex materials whose appearance involves many optical phenomena such as absorption and scattering. They are widely used in work of art and cosmetics among other things, for their colouring power. So, it is of great interest for digital representation to be able to predict the colour of a pigment as a function of shape and size of its particles, or vice versa.

In this work, we have decided to focus on hematite as it is a traditional pigment, whose origin of coloration has been well discussed in the literature [1]. Moreover, we believe that this study can be adapted to any other inorganic pigment.

## Experiments

### Synthesis of Hematite powders

As the preparation of hematite has been widely studied in the literature, it exists a lot of different routes to control the nucleation and growth of  $\alpha\text{-Fe}_2\text{O}_3$  crystallites in solution under standard or hydrothermal conditions. Our study has been done over thirteen samples, chosen to cover a wide range of morphologies and colours, and to mimic the colour variations observed on archaeological rock paintings (Table 1).

	Grain shape	Grain size (nm)	Average crystallite size (nm) $\pm$ anisotropy	Goethite (%m)	Colour [L* a* b*]
4	Sphere	16.0 $\pm$ 2.88	10.9 $\pm$ 0.40	---	[27.1 28.2 22.3]
2	Diamond	20.0 $\pm$ 3.28	20.1 $\pm$ 3.00	---	[27.2 26.2 19.0]
1 <sub>2</sub>	Diamond	24.0 $\pm$ 3.22	25.4 $\pm$ 4.90	---	[25.0 23.2 15.9]
1	Diamond	25.0 $\pm$ 5.90	24.5 $\pm$ 4.80	---	[27.5 27.6 21.6]
6	Diamond	44.0 $\pm$ 7.40	61.2 $\pm$ 10.2	7.17 $\pm$ 0.18	[29.6 23.0 19.7]
5	Diamond	50.0 $\pm$ 8.20	46.3 $\pm$ 8.80	8.98 $\pm$ 0.16	[31.4 26.6 23.3]
AG	Needle	76.2 $\pm$ 23.2	7.30 $\pm$ 3.60	---	[36.2 29.6 31.1]
3	Bi-pyramid	94.2 $\pm$ 10.5 166 $\pm$ 67.0	197 $\pm$ 50.8	---	[32.4 30.3 17.8]
1 <sub>3</sub>	Stick	244 $\pm$ 66.2	206 $\pm$ 43.2	---	[36.2 26.1 16.7]
HT	Platelet	320 $\pm$ 22.8	399 $\pm$ 242	0.91 $\pm$ 0.09	[29.3 24.8 10.6]
P <sub>2</sub>	Ellipsoid	1374 $\pm$ 128	18.3 $\pm$ 0.40	---	[32.7 21.8 7.65]
P <sub>1</sub>	Ellipsoid	1914 $\pm$ 698	16.6 $\pm$ 2.30	---	[32.1 13.7 3.10]
C	Sphere/Stick	98.0 $\pm$ 25.0 4444 $\pm$ 2108	526 $\pm$ 53.3	---	[29.7 12.6 4.47]




Table 1: Features of the hematite crystals (or agglomerates of crystals) and colours of the powders. The samples have been organised by increasing crystallite size. Grain shapes and sizes are determined through SEM images. Average crystallite sizes and mass proportions of goethite are optimised through Rietveld refinements. Colours are calculated from the reflectance spectra in the CIE L\*a\*b\* colour space.

Our samples numbered 1 to 6 have been respectively prepared following the methods 1 to 6 described by [2]. Among these samples, 5 and 6 have been obtained by the transformation of a ferrihydrite precipitate in aqueous suspension under basic conditions. The others have been prepared by forced hydrolysis of  $\text{Fe}^{\text{III}}$  salts solutions in acidic conditions. Only 4 has the particularity to be purified by dialysis. The samples 1<sub>2</sub> and 1<sub>3</sub> are obtained following the same route as 1 using  $\text{FeNO}_3$  and  $\text{FeCl}_2$  respectively as a precursor and with adding an aging of one month after synthesis. The authors also propose a route to obtain purple hematite, but it resulted as goethite  $\text{FeO}(\text{OH})$  which transformed to hematite after being annealed (here 16h at 270°C). It corresponds to the sample 'Annealed Goethite' (AG). This production process is similar to the one of some hematite-based pigments used by

Palaeolithic artists for rock paintings [3-4]. We generated peanuts-like hematite particles  $P_1$  and  $P_2$  following the routes proposed by Sugimoto, Khan and Muramatsu [5], using  $Na_2SO_4$  and  $NaH_2PO_4$  salts respectively. The sample HT has been prepared under hydrothermal conditions following the route suggested by Sugimoto *et al.* [6] for platelet particles. Finally, C is a commercial Iron(III) oxide powder sample purchased from Puratronic®.

### Characterisation

X-Ray powder diffraction (XRPD) data were collected on the dried powders with a Bruker Endeavour D8 diffractometer operated at Cu K $\alpha$  radiation ( $\lambda = 1.5404 \text{ \AA}$ ). DIFFRAC.EVA's (Bruker) search/match module, which performs searches on the PDF4+ (2018) reference database, has been used for phase identification. All analyses of the X-ray powder diffraction patterns were performed with the FP\_Suite software [7]. Rietveld refinements [8] were conducted to obtain the structural and micro-structural parameters of each powder and the mass proportion of hematite and goethite in case of mixture. Morphology (size and shape) of the grains composing the dried samples were studied by scanning electron microscopy (SEM, Zeiss Ultra+ microscope, Néel Institute, Grenoble, France).

The diffuse reflectance of the hematite powders was measured using the spectro-gonio radiometer SHADOWS developed by Potin *et al.* [9]. The measurements were performed on dried powder layer sample sufficiently thick so that the substrate does not contribute to the measured reflectance ( $>1 \text{ mm}$ ), from 400 nm to 1000 nm with a step of 1 nm, with a normal incidence and an observation angle fixed at  $30^\circ$ . We used a Spectralon® as a white reference.

## Results and discussion

### XRPD

Hematite is identified in all of our samples (Figure 1).

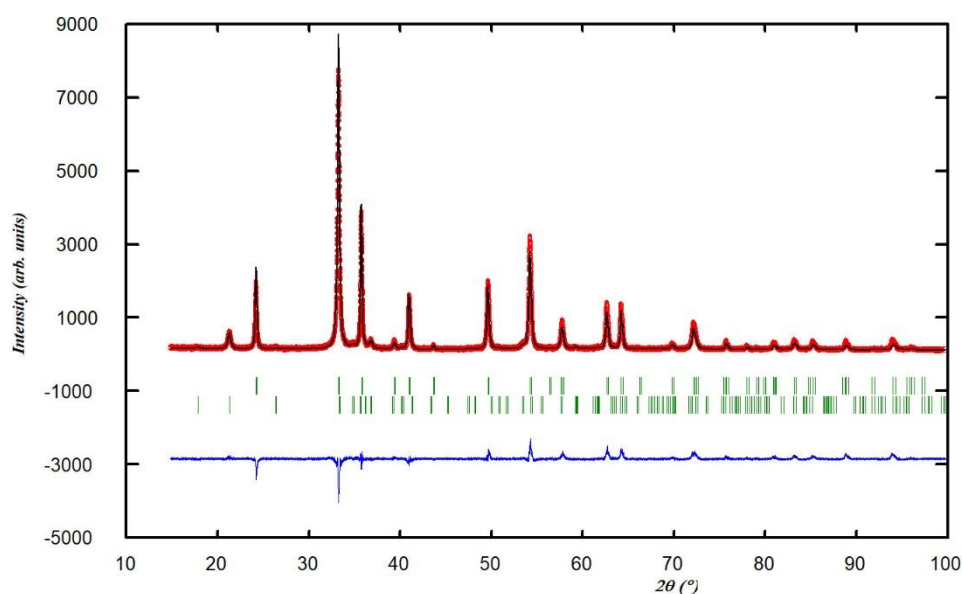
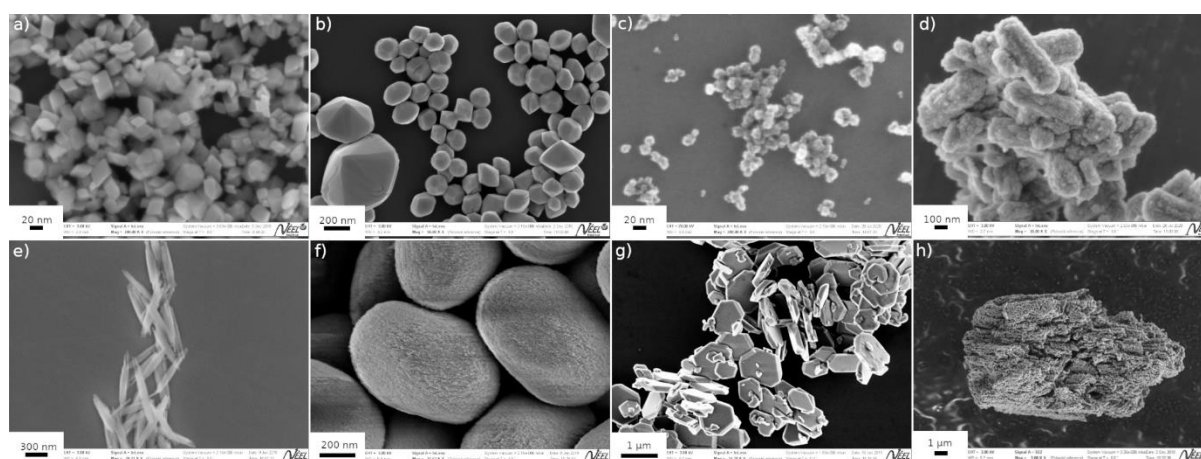


Figure 1: Rietveld refinement results (experimental pattern: red data points, calculated pattern: black full line, difference: blue full line) for samples 5. The vertical ticks indicate the Bragg positions for hematite and goethite respectively.

All samples are pure, except samples 5, 6 and HT, which contain a sufficiently small to be negligible amount of goethite (Figure 1 and Table 1). Crystallographic data and micro-structural parameters have been obtained from the Rietveld powder structure refinement analysis: unit cell parameters, atomic positions/occupancies and average crystallite size. Only the latter parameter seems to significantly distinguish the different samples. It is calculated from the width of diffraction lines and corresponds to the size of domains over which diffraction is coherent. If the powder consists of single-crystals, crystallite size and grain size (entities seen under the microscope) are identical.

### SEM

Except for 3 which is composed of two different size populations (a smaller one  $3_s$  and a larger one  $3_l$ ), the monodispersity of all the samples is well controlled. Various shapes and sizes going from few nanometers to microns are observed (see Figure 2). HT is of big interest because this hexagonal platelet shape is quite similar to the morphology of some natural hematite-based pigment found in Lascaux's painting [10]. 1,  $1_2$ , 2, 5 and 6 all show a diamond shape of different but nanometric sizes. The observed grains also differ from one another from their surface appearance: some of them such as  $P_1$ ,  $P_2$  and  $1_3$  look quite rough. It may also be the case for 4 but the powder is too fine to confirm it. The description of the sample C is quite complex because it can be done at two different scales: small spheres seem to have been annealed so that they melted and assembled to form micrometric grains. The average dimensions of the grains were deduced from SEM images and reduced to only one dimensional parameter per sample by computing the radius of an equivalent sphere. In order to better take into account the shape anisotropy of certain samples (AG and HT), this radius has been computed so that the ratio of the surface over the volume of the grain remains constant. Results are listed in Table 1. Grain size and average crystallite size are in good agreement for all samples: it shows that the powders consist of single-crystals. Larger discrepancies are found for samples AG, C,  $P_1$  and  $P_2$  for which average crystallite size are very smaller than grain size. In this case, grains are therefore agglomerates of small single-crystals, as the SEM image of sample  $P_2$  seems to show (Figure 2f).



*Figure 2: SEM images of the different hematite powders. a) Crystals of samples 1,  $1_2$ , 2, 5 and 6 show pretty similar morphology: same diamond shape and close sizes. Only 1 is shown here. b) Sample 3 presents two bipyramidal shaped crystal populations different in size. c) Sample 4 is composed of very small spherical particles. d) Sample  $1_3$  consists of crystals with a rough surface e) Sample AG (flat needle shape whose thickness is much smaller than its width and its length). f) Samples  $P_1$  and  $P_2$  have the same shape and different sizes. They seem to consist of agglomerates of crystals, forming grains. Only  $P_2$  is shown here. g) Sample HT (large-sized hexagonal platelet shape). h) Sample C presents sticks composed of melted spheres of much smaller size.*

## Reflectance

As all of our samples are quite pure hematite, they all have the same spectral signature: in the studied wavelength range, hematite has three major absorption bands at around 600 nm, 700 nm and 850 nm whose origins are well described by [11], and a fourth one near 430 nm that is too saturated to be of such an interest. Depending on the sample under study, we either note a shift in wavelength, or a change of the intensity, the width and the slope of the bands (Figure 3). To achieve a colorimetric study and visualise the difference between the obtained colours, these spectra are converted into colour coordinates in the CIE  $L^*a^*b^*$  space.

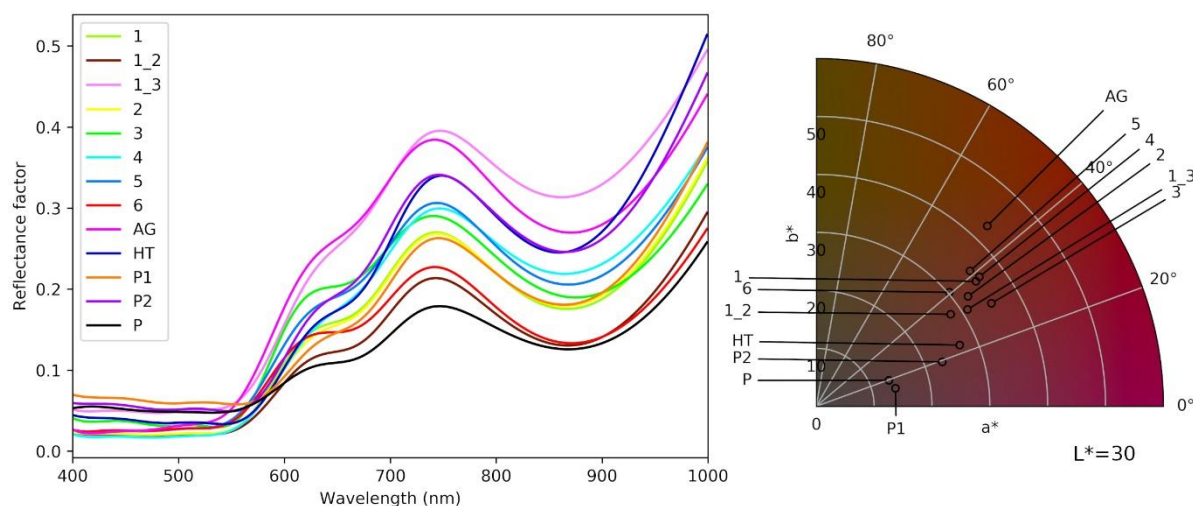


Figure 3: Reflectance spectra of the samples (left), calibrated by a Spectralon®, and position of the corresponding colours in the CIE  $L^*a^*b^*$  diagram for  $L^*=30$  (right).

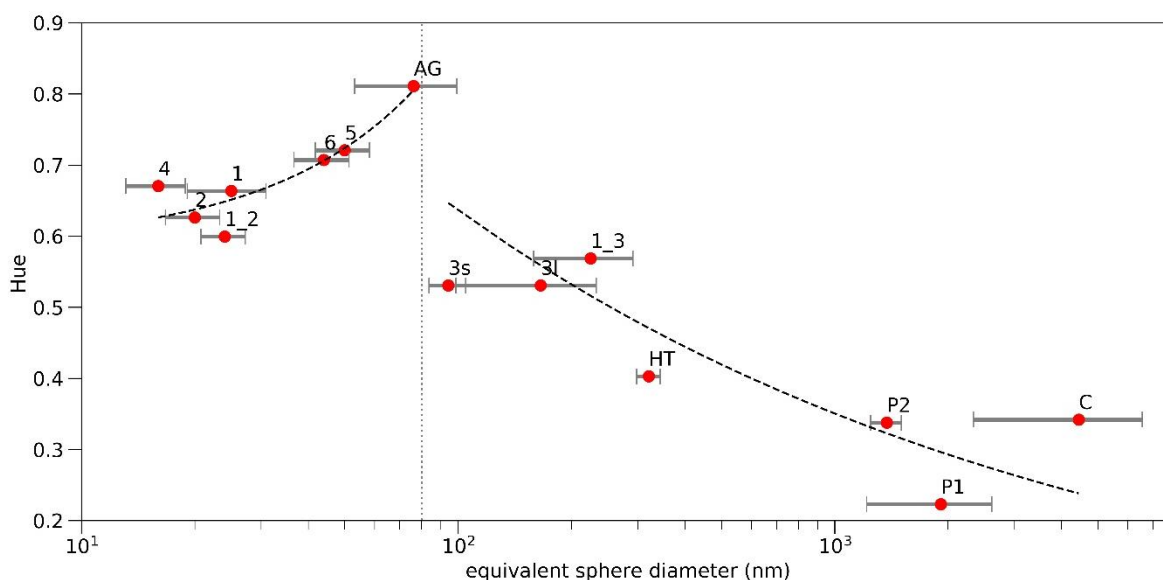


Figure 4: Hue against the equivalent sphere diameter deduced from SEM experiments. The hue is increasing for very small particles until a critical diameter ( $\sim 80$  nm, dot line) where the trend is reversed.

The thirteen syntheses of hematite lead to crystals (or agglomerates of crystals) with different morphologies and/or sizes and to as many powders of different colours that are summarised in Table 1. The micro-structural parameters, spectra characteristics and colour parameters have been studied



alongside with each other to find a correlation between them. In every case, it is possible to distinguish different trends for the very small particles (<80 nm in diameter) and the bigger ones. The most striking results are obtained for the study of the hue against the grain sizes (see Figure 4).

The hue, defined as the angular component of the colour in the polar representation (see Figure 3), is first increasing for small particles, then the trend is reversed after reaching a critical diameter (~80 nm).

There are several physical phenomena that depend on the grain size that are active at this scale. Absorption and scattering are the more important. We tried using scattering models to fit the reflectance spectra. These models rely on the phase function to describe the angular distribution of scattered light. Since the material under study is quite absorbing, we carried our study using the single scattering approximation. We tried three different phase functions: the Mie phase function from exact scattering theory, its approximation for non-absorbing particles small compared to the wavelength (Rayleigh phase function) [12] and the empirical Henyey-Greenstein phase function [13]. The latter has a single parameter,  $g$ , whose value lies between -1 (predominant backward scattering) and 1 (predominant forward scattering). For isotropic scattering,  $g = 0$ . To faithfully describe the observed colour of the powders, we would need a precise measure of the hematite refractive index. Because of the complexity of such a measurement, there are few measures available and they do not fully agree with each other [14-15].

The results of the simulations for the sample 1 are presented in Figure 5. All the cited models lead to an underestimation of the reflectance spectra, regardless of the refractive index value used. As the grain size is much smaller than the wavelength, the Rayleigh theory provides a good approximation of the Mie theory. A more complete modeling would involve the addition of the multiple scattering contribution whose good estimation is proposed by Jensen *et al.* [16]. Nevertheless, as the absorption phenomenon is much stronger, the multiple scattering does not induce a significant improvement in the reflectance simulation.

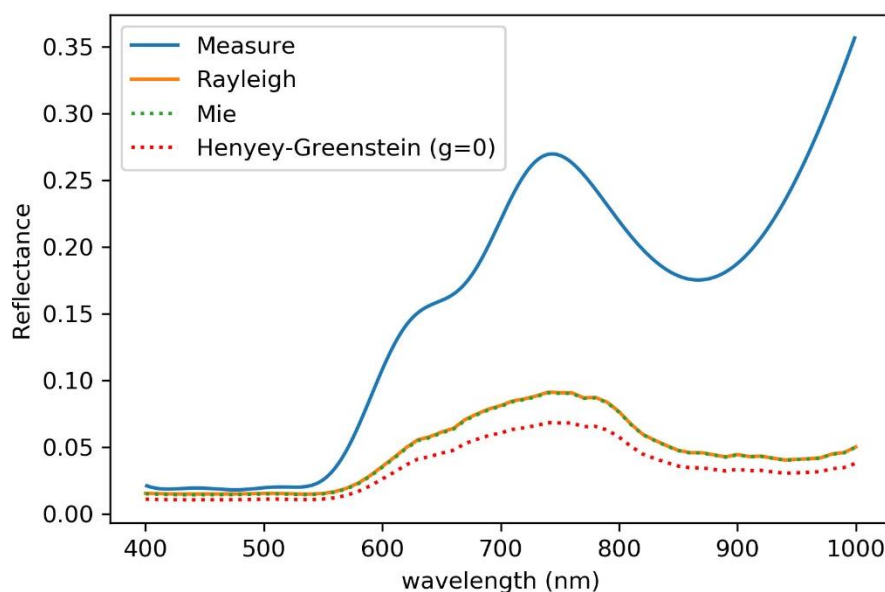


Figure 5: Simulations of the reflectance spectra of sample 1 in the single scattering approximation using the refractive index measured by [14] and different phase functions (Mie scattering, Rayleigh scattering and Henyey-Greenstein scattering).

Other physical phenomena should be taken into account. One major assumption made for the Mie or Rayleigh scattering theory is that the particles are quite dispersed into a host medium. Since dried powders are made of densely packed particles, this assumption is broken in our samples. These models need to be adapted for this specific case. Moreover, the interface between the powder layer and the air is rough so it can induce some surface scattering effect.

## Conclusions

Thirteen nanocrystallised hematite powders showing various morphologies and/or sizes of crystals (or agglomerates of crystals) and a wide range of colours have been synthesised. By comparing the micro-structural features, the characteristics of measured reflectance spectra and the colour parameters in the CIE  $L^*a^*b$  space, it has been observed that some parameters are highly correlated. The study of the hue versus the grain size of the powders shows that the trend following by these parameters is reversed when reaching a critical diameter of about 80 nm. We believe that the influence of different scattering phenomena at stake is changing at this scale causing this change of trend. Simulations of reflectance spectra with well described scattering models are not sufficient to correctly understand the colour of each sample according to the grain size and shape. We will also aim to model the bi-directional reflectance distribution function (BRDF), that would be of great interest for digital representation.

In the future we would like to extend this study to other inorganic pigments, like ochers, mixtures of hematite and clay.

## Acknowledgements

The authors would like to thank Sébastien Pairis and Simon Giraud (Insitut Néel) for their help in the manipulation of the scanning electron microscope, and the chemical syntheses respectively, as well as Corinne Félix (Institut Néel) and Olivier Brissaud (IPAG) for their help in the reflectance measurements. This work was financially supported by the French National Research Agency in the framework of the Investissements d'Avenir program (ANR-15-IDEX-02, Cross Disciplinary Program Patrimialp).

## References

1. Pailhé N, Wattiaux A, Gaudon M and Demourgues A (2008), Correlation between structural features and vis-NIR spectra of  $\alpha$ - $\text{Fe}_2\text{O}_3$  hematite and  $\text{AFe}_2\text{O}_4$  spinel oxides (A= Mg, Zn), *Journal of Solid State Chemistry*, **181** (5), 1040-1047.
2. Schwertmann U and Cornell RM (2008), *Iron Oxides in the Laboratory: Preparation and Characterization*, John Wiley & Sons.
3. Pomies MP, Morin G and Vignaud C (1998), XRD study of the goethite-hematite transformation: application to the identification of heated prehistoric pigments, *European Journal of Solid State and Inorganic Chemistry*, **35** (1), 9-25.
4. Gialanella S, Belli R, Dalmeri G, Lonardelli I, Mattarelli M, Montagna M and Toniutti L (2011), Artificial or natural origin of Hematite-based red pigments in archaeological contexts: the case of Riparo Dalmeri (Trento, Italy), *Archaeometry*, **53** (5), 950-962.
5. Sugimoto T, Khan MM and Muramatsu A (1993), Preparation of monodisperse peanut-type  $\alpha$ - $\text{Fe}_2\text{O}_3$  particles from condensed ferric hydroxide gel, *Colloids and Surfaces A: Physicochemical and Engineering Aspects*, **70** (2), 167-169.



6. Sugimoto T, Muramatsu A, Sakata K and Shindo D (1993), Characterization of hematite particles of different shapes, *Journal of Colloid and Interface Science*, **158** (2), 420-428.
7. Rodríguez-Carvajal J (1993), Recent advances in magnetic structure determination by neutron powder diffraction, *Physica B: Condensed Matter*, **192** (1-2), 55-69.
8. Rietveld HM (1969), A profile refinement method for nuclear and magnetic structures, *Journal of Applied Crystallography*, **2** (2), 65-71.
9. Potin S, Brissaud O, Beck P, Schmitt B, Magnard Y, Correia J-J, Rabou P and Jocou L (2018), SHADOWS: a spectro-gonio radiometer for bidirectional reflectance studies of dark meteorites and terrestrial analogs: design, calibrations, and performances on challenging surfaces, *Applied Optics*, **57** (28), 8279-8296.
10. Chalmin E, Menu M, Pomiès MP, Vignaud C, Aujoulat N and Geneste JM (2004), Les blasons de Lascaux, *L'anthropologie*, **108** (5), 571-592.
11. Pailhé N, Wattiaux A, Gaudon M and Demourgues A (2008), Impact of structural features on pigment properties of  $\alpha$ -Fe<sub>2</sub>O<sub>3</sub> haematite, *Journal of Solid State Chemistry*, **181** (10), 2697-2704.
12. Bohren CF and Huffman DR (2008), *Absorption and Scattering of Light by Small Particles*, John Wiley & Sons.
13. Henyey LG and Greenstein JL (1941), Diffuse radiation in the galaxy, *The Astrophysical Journal*, **93**, 70-83.
14. Querry MR (1985), Optical constants, *Contractor Report Sep 1982 - May 1984*, Missouri University, Kansas City (USA).
15. Couka E, Willot F, Callet P and Jeulin D (2015), Optical response of a hematite coating: ellipsometry data versus Fourier-based computations, *Advanced Science, Engineering and Medicine*, **7** (11), 925-931.
16. Jensen HW, Marschner SR, Levoy M and Hanrahan P (2001), A practical model for subsurface light transport, *Proceedings of the 28<sup>th</sup> Annual Conference on Computer Graphics and Interactive Techniques*, 511-518, Los Angeles (USA).